Surface Force Arising from Adsorbed Graphene Oxide in Alumina Suspensions with Different Shape and Size

Hazlina Husin
School of Mechanical and Chemical Engineering, The University of Western Australia, Crawley 6009, Australia

Faculty of Chemical Engineering, Universiti Teknologi MARA, Shah Alam 40450, Malaysia

Yee-Kwong Leong and Jishan Liu
School of Mechanical and Chemical Engineering, The University of Western Australia, Crawley 6009, Australia

Hyoung Jin Choi and Wen Ling Zhang
Dept. of Polymer Science and Engineering, Inha University, Incheon 402-751, Republic of Korea

DOI 10.1002/aic.14133
Published online May 21, 2013 in Wiley Online Library (wileyonlinelibrary.com)

The effects of graphene oxide (GO) on the yield stress-pH of α-Al_2O_3 (alumina) suspensions were investigated. For micron-sized platelet alumina suspensions, micron-sized GO additive increased the maximum yield stress by as much as six-folds. This was attributed to GO-mediated bridging interactions between the platelet particles. This type of bridging interactions was much less effective with submicron-sized, spherical, and irregular shape alumina. Adsorption of the anionic GO reflected by the shift of pH of zero zeta potential to a lower pH is particularly high for platelet alumina. The 1.0 dwb % GO concentration added is sufficient to reinforce each platelet particle–particle bond, assisted by a directed GO–platelet interaction configuration. This is, however, not true with submicron-sized particles as the particle concentration increases sharply with the inverse of the particle diameter to power of 3. Moreover, a GO sheet can adsorb several submicron-sized particles and this does not produce the right interaction configuration. © 2013 American Institute of Chemical Engineers *AIChE J*, 59: 3633–3641, 2013

Keywords: graphene oxide, alumina morphology, yield stress, zeta potential, particle bridging

Introduction

The use of yield stress parameter to characterize the interparticle forces in suspension has revealed fundamental understandings on the relationship between intermolecular and intramolecular forces and the molecular structure of adsorbed additives. This is because these molecular forces affect differently the strength of attraction between particles in three-dimensional (3-D) flocculated network. In the past 20 years, our group has focused on understanding the relationship between adsorbed additives molecular properties such as structure, architecture, functional group types, location and quantity, and the nature and strength of the surface forces in suspensions. Now, we are extending this study to interparticle forces arising from "large" flat molecules with edge-located charged functional groups, that is, graphene oxide (GO), in suspensions of α-Al_2O_3 (alumina) with different shaped particles; irregular, spherical, and platelet.

Graphene, a large single-layer graphite molecule, has attracted considerable interest in the research sphere recently[1–4] due to its excellent electrical conductive, thermal, adsorbent, structural, and mechanical properties.[5–7] Its potential applications are very wide ranging. It has been studied as resonator, solar cell, supercapacitor, battery, catalysts support, hydrogen storage and adsorbent, and composite materials.[8–14] GO is an oxidized form of graphene while still retaining its sheet structure. GO is a continuous sheet of interlinking benzene rings with components of oxygenated functional groups located on the basal face and edge. GO is, therefore, relatively hydrophilic and will interact well with water. Studies revealed that functional groups such as polar carbonyl, hydroxyl, and epoxide groups are present and located on the edges and basal plane of the GO sheet.[15–17] Some research groups believed that carboxylic acid groups are also present but are located only at the edges of the sheet.[17] Galande et al.[18] reported that due to the carboxylate group, there is a presence of high negative density at the edge of the GO sheet using computer-modeled structure and fluorescence spectroscopy determinations. These functional groups, however, interrupt the conjugation of sp^2 network in the interlinked benzene rings segment[19] and hence GO is considered as a poor electric conductor.[20] The conductivity of GO is lower (6×10^{-6} Scm^{-1}) than that of graphite (6.7×10^2 Scm^{-1}).[21]

Recently, electroresponsive of GO-based composites, for example GO/polyaniline,[21] GO/titania (TiO_2),[22] and GO/polystyrene,[23] showed that dispersed GO-based composite particles in silicone oil form chain-like structures under

Correspondence concerning this article should be addressed to Y.-K. Leong at leong@mech.uwa.edu.au.

© 2013 American Institute of Chemical Engineers

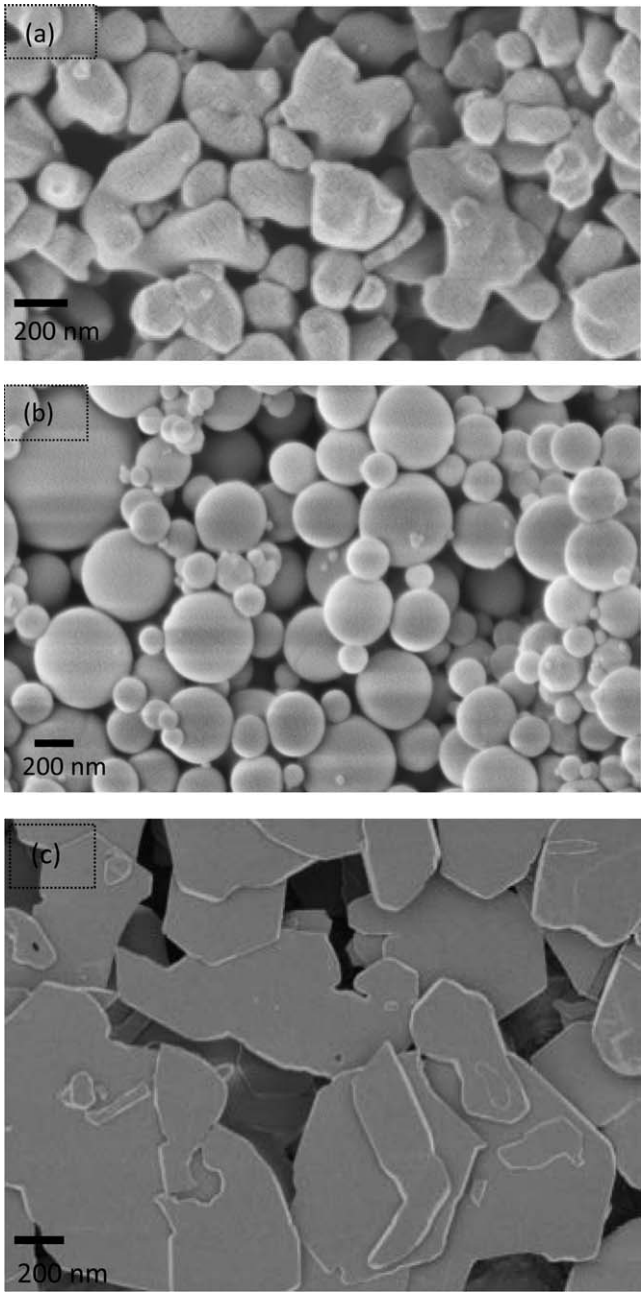

Figure 1. SEM images of (a) irregular AKP30, (b) spherical AO802, and (c) platelet Alusion alumina powders used in this study.

external electric field. Zhang et al.[23] reported the presence of a yield stress at the zero-shear rate limit for these suspensions under an applied electric field. This yield stress was found to vary linearly with the square of electrical field strength. In this study, we evaluate the surface forces arising from adsorbed GO in aqueous alumina suspensions (no electric field is applied) at the pH of maximum yield stress and correlate these surface forces with the GO structure and morphology of the alumina particles. Usually, the pH of maximum yield stress is located at the pH of zero zeta potential.[24–26] At this point, only the van der Waals attractive force is responsible for the strength of particle–particle attraction in the 3-D network structure provided that no adsorbed additive is present.[26] Otherwise, one or more of the non-DLVO (Derjaguin-Landau-Verwey-Overbeek) forces such as steric, bridging, and hydrogen bond, will also be present depending on the molecular properties of the additives.[24,25,27] So, by evaluating the change in the maximum yield stress in suspension with GO-mediated particle interactions, we can deduce the prevailing non-DLVO forces operating. The nature and strength of the surface forces interacting between particles control suspension properties and behavior in the products and in processing such as in flow, mixing, sedimentation, flotation, aggregation, and others. Hence, there is a continual search of additives with the ideal molecular properties to optimize suspension processing and behavior and this report is one such study.

Materials and Methods

GO powders were prepared via a modified Hummers[28] method from pristine graphite powders [flake, ~20 μm, 100 mesh ($\geq$75% min), Sigma-Aldrich]. Graphite powders, reagent $KMnO_4$ (Sigma-Aldrich), and reagent $NaNO_3$ (Junsei, Japan) were added gradually to H_2SO_4 (98%, DC Chemical, Korea). The mixture was stirred vigorously for 3 h until graphite oxide was yielded. The graphite oxide was treated with a 30% H_2O_2 solution until its color turned into vivid brown indicating the formation of fully oxidized graphite. The as-obtained graphite oxide slurry was exfoliated to generate GO sheets by sonication at 60°C, for 1 h using an ultrasonic generator (28 kHz, 600 W, Kyungil Ultrasonic, Korea). Finally, the mixture was separated by centrifugation, washed copiously with 5% HCl, and deionized water until it reached pH 7; and dried in a vacuum oven at 60°C for 24 h. According to Malvern Mastersizer, the prepared GO has an equivalent spherical particle size of 27.85 μm. The GO sheets are relatively hydrophilic. It was found that water molecules are strongly hydrogen bonded to the epoxide and hydroxyl groups on its basal plane.[17]

Three different shape of α-Al_2O_3 (alumina) powders were used; irregular, spherical, and platelet. The irregular-shaped powder known as AKP30 was purchased from Sumitomo Chemical Company (Japan). The spherical powder AO802 was provided from Admatech (Japan) with a mean-particle size specification of 0.7 μm. The platelet powder known by its trade name of Alusion, was sourced from Advanced Nanotechnology Limited, now known as Antaria (Perth, Australia). This powder is commonly used in cosmetics as it produces a soft-focus optical effect.[27] The scanning electron microscope (SEM) images of these powders obtained via a Zeiss 1555 VP-FESEM SEM are shown in Figure 1. Properties of these powders such as particle-size distribution (d_{10}, d_{50}, and d_{90}), BET surface area, density, and isoelectric point are tabulated in Table 1. The median size, d_{50}, of AKP30 and AO802 are submicron-sized, that is, 0.34 and 0.4 μm, respectively,

Table 1. Morphology of Alumina AKP30, AO802, and Alusion Used in This Study

	Alumina–AKP30	Alumina–AO802	Alumina–Alusion
d_{10}	0.13 μm	0.15 μm	4.78 μm
d_{50}	0.34 μm	0.40 μm	9.43 μm
d_{90}	2.96 μm	1.26 μm	15.43 μm
BET surface area	6.4 $m^2\ m^2\ g^{-1}$	4.9 $m^2\ m^2\ g^{-1}$	1.8 $m^2\ m^2\ g^{-1}$
Average particle density	3920 kgm^{-3}	3650 kgm^{-3}	3970 kgm^{-3}
Isoelectric point (*pI*)	~9	~8.5	7–-8

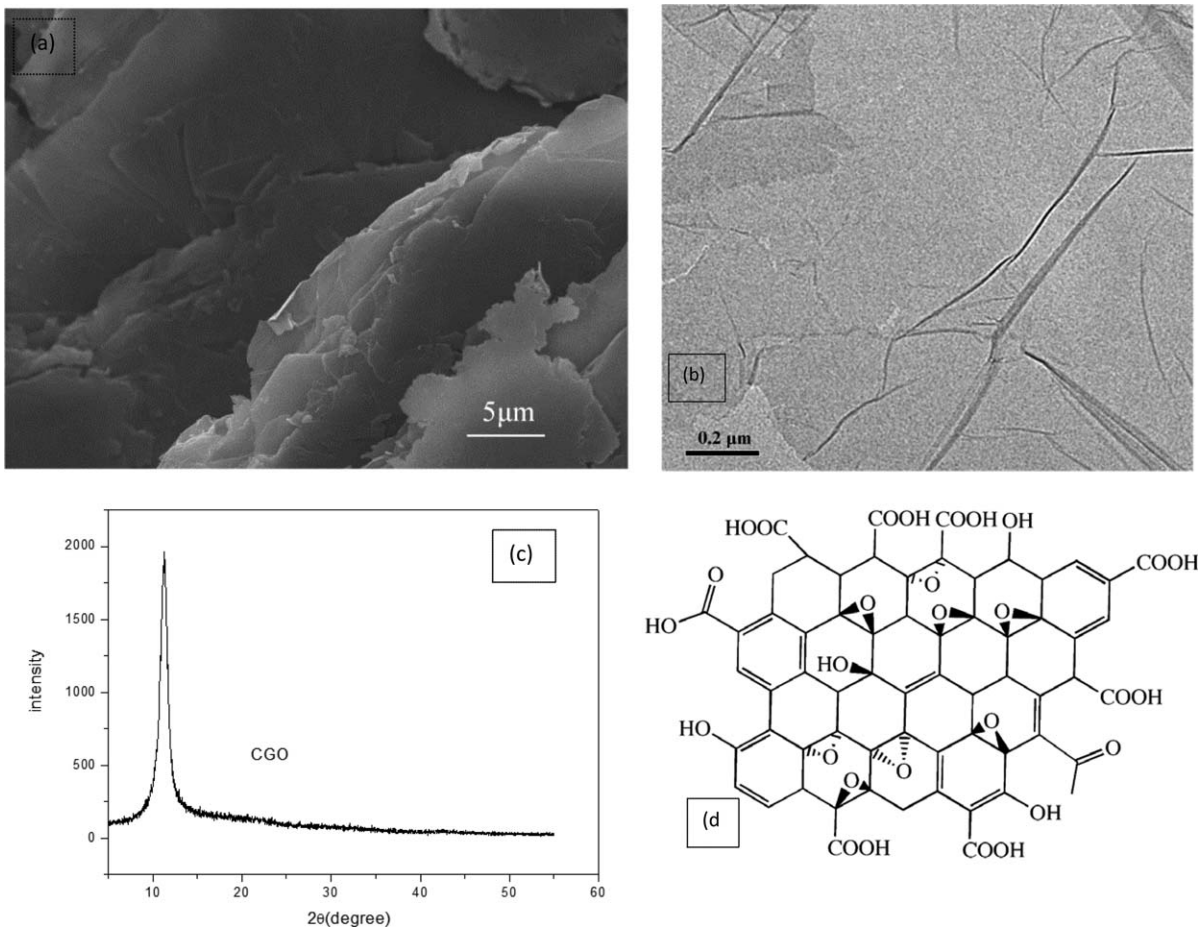

Figure 2. The morphology of GO analyzed using (a) SEM image (b) TEM image, (c) its XRD spectrum, and (d) the structural model of GO.[30]

whereas the platelet Alusion alumina is an order of magnitude larger. The Alusion particles are micron-sized like the GO, that is, 9.43 μm for the median size. At a given solids concentration, the particle concentration will be much larger for the finest particle suspensions. The isoelectric point (IEP) of the three powders varied over a narrow pH range of 7–9 with the Alusion alumina suspension having the lowest value. With the submicron-sized AKP30 and AO802 powders, multiple particles adsorption on GO sheet is likely as in the case of SiO_2[20] and TiO_2.[22] When the particle size is larger than the GO sheet, it is possible to have a few GO sheets adsorbed on a particle.[23] The size of Alusion platelet sheet is, however, slightly smaller than the GO sheet.

Yield stress and zeta potential measurements were conducted on alumina suspensions, with and without the presence of GO. For the yield stress measurement, concentrated alumina slurry containing 55 wt % solids was prepared. GO powder was first suspended in distilled water by bath sonification for 24 h. Then, a few drops of concentrated NaOH ($\sim$5 M) were added to increase the pH to $\sim$8, followed by alumina powder. The mixture was vigorously stirred until homogenous slurry was obtained. The slurry was left to rest for $\sim$5 min. During the measurement, concentrated HNO_3 (5 M) was used to decrease the pH of the slurry. Only concentrated NaOH or HNO_3 ($\geq$5 M) was used in the experiment to avoid dilution. At each pH interval, the sample was agitated with a spatula prior to measurements of pH and yield stress.

For the zeta potential measurement, the aforementioned steps were repeated for preparation of dilute alumina slurry of 5 wt % solids. The mixture was sonicated (Branson Digital sonifier, 50% amplitude), left to rest for $\sim$5 min and its zeta potential was measured with a ZetaProbe (Colloidal Dynamic) as a function of pH. Like the yield stress measurements, the direction of the zeta potential measurements was from high to low pH using 0.5 M HNO_3 solution to change the pH automatically and in a control manner by the machine.

Results and Discussion

Figures 2a, b showed the distinctive sheet structure of GO identified by SEM with an applied voltage of 15 kV at a work distance of 15 mm (SEM, S-4300, Hitachi, Japan) and by transmission electron microscope (TEM; Philips CM200). According to Figure 2b, the lateral dimension of GO used in this study is $\sim$1.2 μm. The crystal structure of GO was identified by x-ray diffraction (XRD) (DMAX-2500, Rigaku) in Figure 2c displaying a typical peak[21,23,29] at $2\theta = 10.88^\circ$. Figure 2D showed the molecular structural model of GO.[30]

During the preparation of GO suspension, GO powder was added to the distilled water forming a dark color liquid as shown in Figure 3. This color liquid was similar to what has been reported by others.[17,31] No particulate material was visible which indicates that the GO sheets were fine in size and well-dispersed. The ease of complete dispersion is

Figure 3. GO suspension in distilled water obtained by bath-sonication.

consistent with the hydrophilic properties of GO. Others had reported similar ease of dispersibility of GO in water via sonication and even simple stirring.[31] The GO-water mixture was quite acidic with a pH of 2.73 and 2.76 at 0.5 dwb % (g GO per 100 g alumina-without the alumina particle) and 2.35 and 2.47 at 1.0 dwb % concentration. The higher acidity of the suspension at high GO concentration indicates the presence of a relatively strong acidic group such as —COOH. The presence of —COOH group in GO is still in dispute among members of this research community.[17] The pH values obtained in this study are much lower than that reported by Galande et al.,[18] which is 5.2 but the GO concentration employed was unspecified.

In a very recent paper, Konkena and Vasudevan[32] reported the data for zeta potential, concentration of ionized groups, and charge density in the pH range of 2–11 for GO prepared by the same Hummers' method employed here. GO was found to be negatively charged through the whole pH range. The negative charge density at pH 2 remained quite significant, slightly more than 20% of that at pH 11, the fully charged state. The ionized group concentration is also relatively high, 10% of that at pH 11 and 12. The magnitude of the negative zeta potential decreased with decreasing pH; −54.3 mV at pH 10.3 to −15 mV at pH 2. A similar variation of the zeta potential with pH for fine and coarse GO synthesized using the same method was reported by Wang et al.[33] The trend of the variation of the zeta potential with pH is the same for both the fine and coarse GO. However, the negative zeta potential for the fine GO is larger than the coarse GO at any given pH. For example, at pH 2, the zeta potential is −22 mV compared to −7mV for the coarse GO. This larger negative zeta potential explained the greater stability of the fine GO sheets at pH 4 and the instability or flocculation of the larger GO sheets at the same pH. The larger negative zeta potential of the smaller GO was attributed to its larger edge charge density to sheet surface area ratio.

For adsorbed additive-mediated particle–particle interactions, the maximum yield stress of the suspension may increase or decrease. An adsorbed additive is regarded as a good steric agent if it brings about a very large reduction in the maximum yield stress. Reduction by as much as 70% has been reported.[24,25] At the other extreme where it increases the maximum yield stress by several folds, it is regarded as a very good particle-bridging agent.[34] Whether an additive is a good steric or bridging agent is determined by its molecular properties.[27,34–37] Figures 4a–c show the yield stress-pH behavior of the AKP30, AO802, and Alusion alumina suspensions. For the pristine suspensions, that is, without added GO, the maximum yield stress generally decreases with median particle size, that is, AKP30 > AO802 > Alusion alumina suspensions at the same solids concentration. The maximum yield stress is 330, 110, and 32 Pa for AKP30, AO802, and Alusion suspensions, respectively. The maximum yield stress is located at pH 9, 8.5 and 8, respectively.

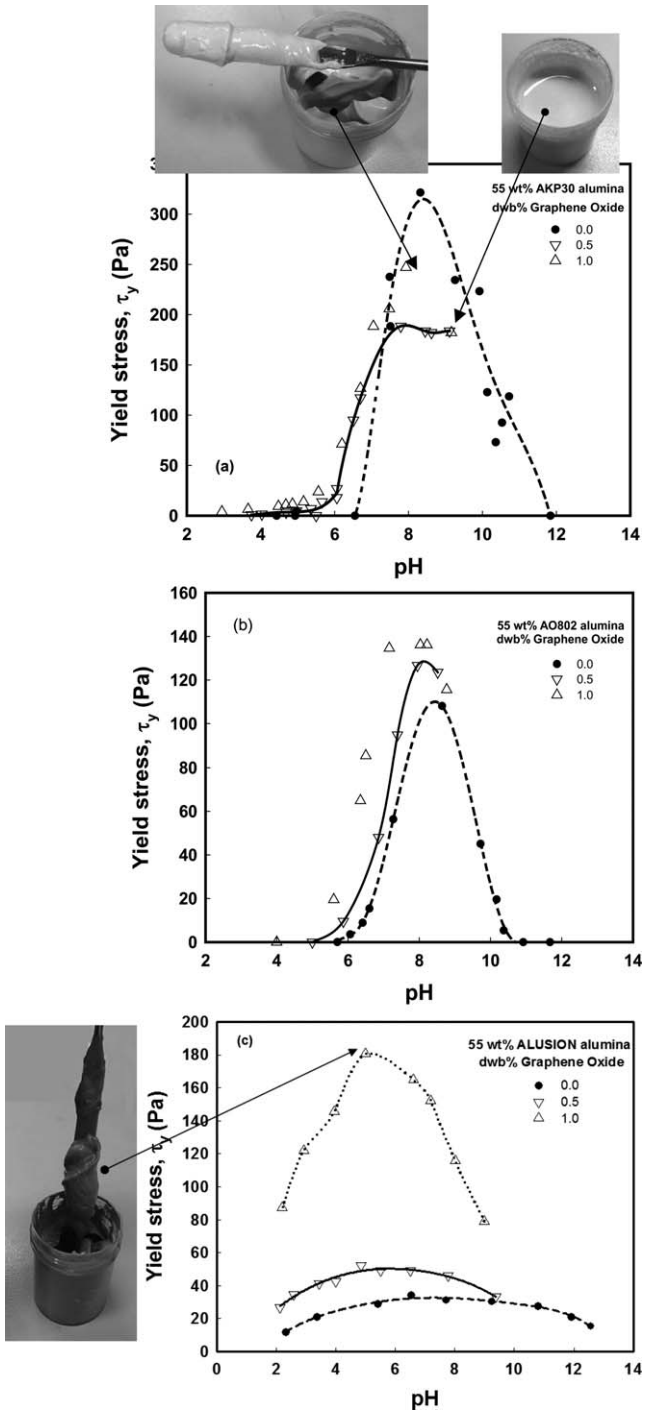

Figure 4. The effect of GO on yield stress-pH behavior of (a) irregular AKP30, (b) spherical AO802, and (c) platelet Alusion alumina suspensions.

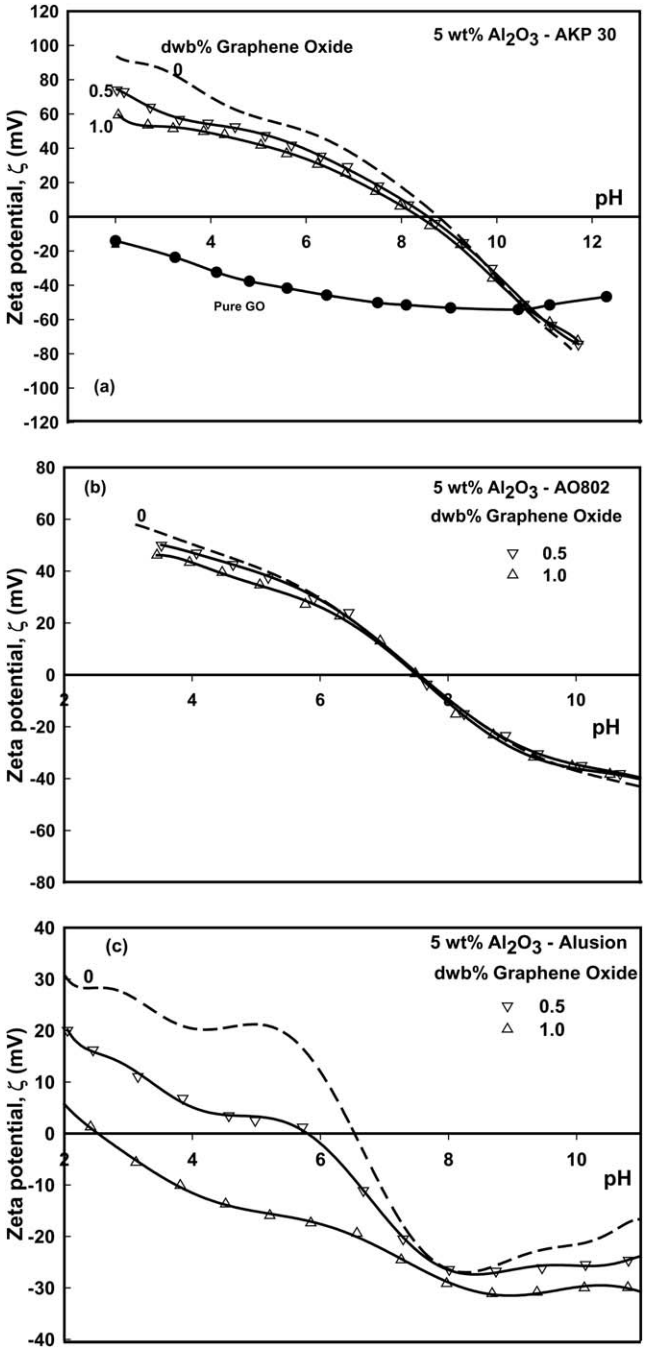

Figure 5. The effect of GO concentrations on zeta potential-pH behavior of (a) irregular AKP30, (b) spherical AO802, and (c) platelet Alusion alumina suspensions.

The zeta potential-pH data for pure GO shown in (a) were sourced from Konkena and Vasudevan.[32]

In the presence of GO, the maximum yield stress of AKP30 alumina suspension was reduced to 185 and 250 Pa at 0.5 and 1.0 dwb %, respectively, as shown in Figure 4a. This represents a 44 and 24% reduction. In contrast, the maximum yield stress of AO802 alumina suspension was increased to 130 and 140 Pa at the same concentrations representing a 1.2-folds and 1.3-folds increase, respectively, which can be seen in Figure 4b. The maximum yield stress is located at pH 8 and 7.5 for 0.5 and 1.0 dwb % GO, respectively. GO produced a much more dramatic increase in the maximum yield stress for Alusion alumina suspension. The increase was almost an order of magnitude higher as shown in Figure 4c. Also, the suspension remained flocculated over the entire pH range from 2 to 9 with and without GO. The maximum yield stress was increased to 50 and 180 Pa at 0.5 and 1.0 dwb %, respectively. This reflects a 1.6-folds and 5.6-folds increase located at pH 6 and 5.5, respectively.

The zeta potential characterizing the alumina surface properties in the suspensions with and without GO has been characterized. Zeta potential is affected by pH and the extent of the ionic additive adsorption. Adsorbed anionic additive such as GO should typically shift the pH of zero zeta potential ($pH_{\zeta=0}$) to a lower value.[24,25] The extent of the shift is dependent on the GO concentration and the amount of GO relative to the total particle surface area. For very high specific surface area particles, a higher amount of adsorbed GO is required for the same extent of shift. Figure 5 shows the effect of GO concentration on the zeta potential-pH behavior of the AKP30, AO802, and Alusion alumina suspensions. The zeta potential-pH data of pure GO taken from Konkena and Vasudevan[32] were also plotted in Figure 5a clearly showing its anionic characteristics. The $pH_{\zeta=0}$ shift by GO is quite small for AKP30 as shown in Figure 5a. At 0.5 and 1.0 dwb % GO, the shift is only 0.2 and 0.4 pH unit for AKP30 suspensions which is within the noise level of the zeta potential measurement. However, at lower pH, the difference in the zeta potential is more pronounced and the zeta potential is smaller in value indicating the presence of GO adsorption. The $pH_{\zeta=0}$ shift is even more insignificant for AO802 suspension by GO as shown in Figure 5b. At lower pH, the zeta potential-pH curves began to deviate with the higher GO content suspension displaying a lower positive zeta potential. This again is an indication of the presence of GO adsorption. This insignificant $pH_{\zeta=0}$ shift or minimal reduction of zeta potential in the low pH region may implies that either no GO or only a small amount of GO has been adsorbed onto the alumina particles. Note that it is possible for the degree of GO adsorption to be high but its total negative charge is small compared to the amount of positive charge in the high specific surface area alumina particles. In contrast, the shift in the $pH_{\zeta=0}$ and the reduction in the zeta potential in the low pH region are more pronounced for the platelet Alusion alumina suspensions as shown in Figure 5c. At 0.5 dwb % GO, the shift is 0.8 pH unit. This is four times the shift observed with AKP30 suspension. At 1.0 dwb % GO, the shift is even greater, 4 pH units. The platelet alumina particle is relatively large with a much lower specific area as shown in Table 1. Its specific area is more than three times smaller as compared to AKP30. This means that a smaller amount of adsorbed GO should produce a more pronounced $pH_{\zeta=0}$ shift. The large shift in $pH_{\zeta=0}$ may also indicate a high degree of GO adsorption. The onset of GO adsorption appeared to be located at pH 6.5 from the Figure 5c where the alumina particles begin to acquire a net positive surface charge. This is accompanied by a reduction in the zeta potential from 0 to -20 mV on GO adsorption. Note that the isoelectric point of the Alusion suspension shown in Figure 5c is located at pH $\sim$7 which is a pH unit lower to another batch of Alusion suspension reported earlier.[27]

The larger yield stress displayed by the finer suspensions is due to the sharp increase in the particle number concentration at a given solids concentration. This concentration

increases with the inverse of the particle size to the power of 3. Despite the van der Waal forces of attraction being weaker for interaction between finer particles, the higher concentration of particle–particle interactions more than compensate for this negative impact resulting in a higher maximum yield stress or viscosity. Leong et al.[26] had shown the importance of particle concentration on the maximum yield stress at the isoelectric point for a range of oxide suspensions.

The decrease and increase in the maximum yield stress of AKP30 and AO802 alumina suspensions by GO indicates the presence of GO adsorption despite the relatively weak zeta potential results. We have observed similar weak zeta potential results with other adsorbed additives such as benzoic acid derivatives, with the second functional group being another —COOH or —OH group[36,37] and bolaform compounds with two –—COOH groups.[34] These additives, however, produced a very large effect on the maximum yield stress of the suspensions.

The maximum yield stress reduction of AKP30 alumina suspensions (Figure 4a) indicates that the particle network strength is weakened by GO. This could occur via two means; the added GO (1) disrupts the network structure and (2) act as a steric barrier thereby weakening the van der Waal interparticle attractive force by keeping the interacting particles further apart. The particle-size distribution of these AKP30 suspensions was, therefore, measured. It was found that the size was much coarser in the presence of GO. The d_{10}, d_{50}, and d_{90} were 0.18, 0.93, and 3.57 μm for suspension with 0.5 dwb % GO and 0.32, 1.34, and 3.26 μm for suspension with 1.0 dwb % GO. The size distribution for the pristine suspension is tabulated in Table 1, which showed a much smaller d_{50} of 0.34 μm. The increase in the particle size is consistent with a GO sheet having a few submicron alumina particles adsorbed on it like that reported earlier between GO and SiO_2[20] and TiO_2.[22] These composite particles may disrupt the network structure weakening it instead.

Meanwhile, the increase in the maximum yield stress of both AO802 (Figure 4b) and Alusion (Figure 4c) alumina suspensions by GO indicates the presence of an additional attractive force such as bridging. Like AKP30, GO increased the median size of the AO802 suspensions. The d_{50} is 1.97 and 1.80 μm for the suspension with 0.5 and 1.0 dwb % GO. Unlike AKP30, the presence of these composite particles in this case strengthened the network slightly. However, in the case of Alusion suspension, the size distribution was not affected by GO. The d_{10}, d_{50}, and d_{90} were 4.58, 9.61, and 16.49 μm for the platelet alumina suspension without GO, 4.67, 9.97, and 16.62 μm for the 0.5 dwb % GO and 4.36, 9.31, and 15.59 μm for the 1.0 dwb % GO. The platelet alumina particles are as large as the GO sheets and so it does not take much energy to separate the adsorbed GO sheets from the particles. A simple mechanical stirring is enough to hydrodynamically force them apart. At the pH of maximum yield stress of 5.5 for the platelet alumina suspension with 0.5 dwb % GO, almost all the carboxylic acid groups will be charged according to the average pKa value of 4.8 for the carboxylic group. The relatively small rise in the maximum yield stress at this pH suggests that not all the particle–particle bonds in the flocculated network were mediated by adsorbed GO probably due to insufficient GO being available. The very large increase of 5.6-folds by 1.0 dwb % GO suggests that every particle–particle bond in the network being reinforced by adsorbed GO.

Between pH 2 and 5.5, the yield stress of Alusion alumina suspensions in the presence of GO is still higher than the pristine suspension. The yield stress showed a decreasing trend from pH 5–2. This means that particle bridging contribution to the yield stress by adsorbed GO diminished with decreasing pH and this is expected. Konkena and Vasudevan showed that the charge density, concentration of ionized groups, and the magnitude of the negative zeta potential decreases with decreasing pH. At pH 2, the charge density is only 20% of the total charge density. As the strength of particle bridging bond is directly linked to the number of charge groups on the GO edge being bonded to the oppositely charged particle surface groups, a smaller concentration of charged group or ionized group, 10% at pH 2, would, therefore, lead to generally weaker particle-bridging interaction. This explained the decreasing yield stress from pH 5.5–2. Wang et al.[33] reported that smaller GO sheets is more stable at low pH 4 where the larger GO will precipitate out. Our previous studies with weak acidic additives such as citric acid showed that once adsorbed it remains adsorbed even at very low pH[35] despite its solution state charge being net neutral. In all our previous studies with anionic additives, the suspensions were prepared at an alkaline pH and the so the adsorption commenced at a relatively high pH and became very significant at pH below the isoelectric point of the particles. For the large GO sheets that were displaced into the solution due to the lack of edge charges for surface anchoring, flocculation between the sheets can occur. However, the van der Waals force responsible for the flocculation is expected to be relatively weak because of its relatively low carbon atom density and the larger sheet separation distance due to its surface epoxide groups keeping the sheet further apart. Even attraction between graphene sheets is relatively weak as reflected by its ease of separation such as via the scotch tape method.

There are many possible configurations of the GO-mediated bridging interactions between alumina platelets. The carboxylic groups located only at the edges of the GO sheets could bind two platelet alumina particles in a face–face, edge–face, or edge–edge configuration in the network structure. Figure 6 shows a schematic diagram of (a) edge–face and (b) edge–edge GO-mediated bridging. The separation distance between interacting particles by GO sheets can be quite large, that is, the length or the width of the sheet. In this case, the van der Waals interaction between the particles should be relatively weak. The network structure in the suspension must, therefore, derived most of its strength from this heterogeneous charge attraction between GO and platelet alumina. A GO sheet will have four edges and so it can acts as a source of network junction in the suspension. A GO sheet junction will have several particles bind to its edges via a mixture of edge and face attachments. Note that the adsorption bond formed between the GO and alumina surface is a negative–positive charge attraction.

As GO produced a very large increase in the yield stress of Alusion alumina suspensions at all pH level, a plausible GO-mediated bridging model explaining this behavior is greatly warranted. However, the GO-mediated particle bridging interaction can only occur in the manner described in Figure 6 if the edge charged groups are responsible for the particle bridging. At pH above isoelectric point, greater than

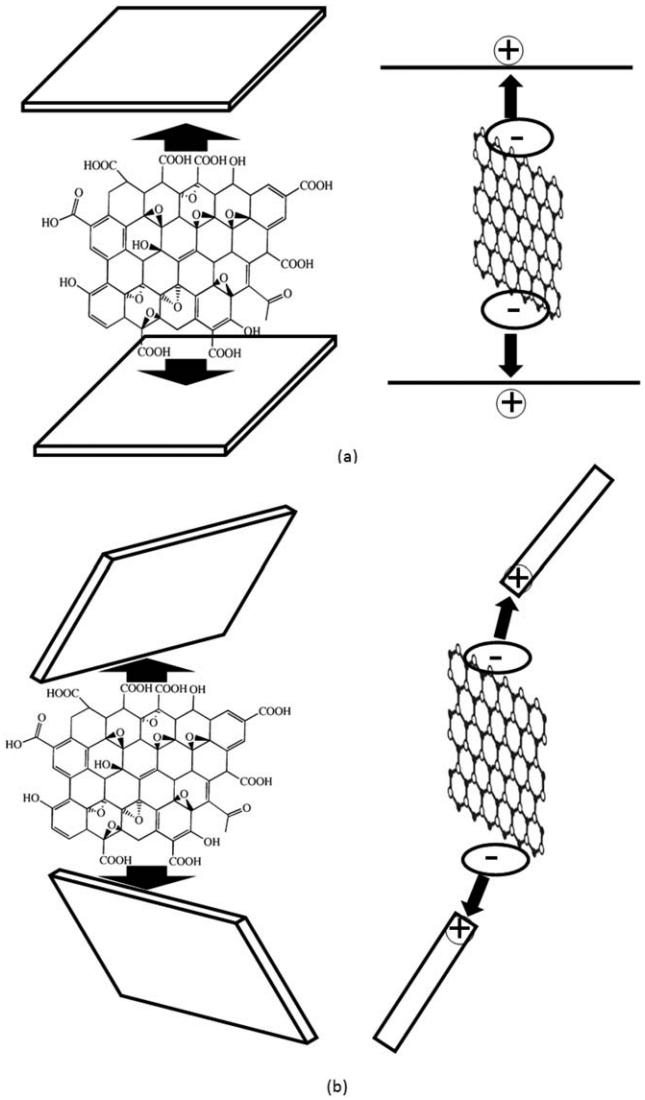

Figure 6. Proposed bridging interaction between the carboxylate groups located on the edge of the GO sheets and particles via (a) edge–face, or (b) edge–edge interaction.

pH 7.5 for Alusion alumina, the particle charge is net negative, and so the extent GO adsorption is smaller and hence a weaker bridging effect was observed. At pH below the IEP, $pH < 7$, the charge density is positive and increases with decreasing pH. GO adsorption should be high and bridging effects should become more important. As a result, we observed a large maximum yield stress at pH $\sim$ 5. At very low pH, the negative edge charge density of GO decreased producing a much weaker particle-bridging interaction despite a much larger positive charge density of alumina particles. Because the particle bridging is due to heterogeneous charge attraction, it is possible that the yield stress-DLVO force model being obeyed by these suspensions.

One of the yield stress-DLVO force models used to explain particle–particle interactions is given by Eq. 1[38,39]

$$\tau_y \approx \frac{\phi^2}{a}\left(\frac{A}{12D_o^2} - \frac{C}{D_o}\zeta^2\right) \quad (1)$$

where τ_y is the yield stress, D_o the separation distance between two particles, ϕ the solids volume fraction, a the particle size, A the Hamaker constant of the particle in water, and ζ the zeta potential. $C = 2\pi\varepsilon_w \ln((1-\kappa D_o)^{-1})$ where ε_w is the permittivity of water and κ the inverse of the debye layer thickness. If the model is obeyed, then the yield stress should decrease linearly with the square of the zeta potential where for many suspensions this has been the case.[39–41] Generally, the yield stress of most suspensions does not scale to ϕ^2. In the presence of adsorbed additive, the minimum separation distance between two interacting particles in the flocculated state will be increased by the adsorbed layer. This means a weaker van der Waals force which is typically reflected by a reduction in the yield stress. In the case where additive layer thickness is not constant, this model is not obeyed.[42] The yield stress vs. zeta potential square plots for AKP30, AO802, and Alusion are shown in Figure 7. The pairing of the yield stress and zeta potential was made at the same surface chemistry condition, that is, making the pH of maximum yield stress equal to the pH of *pI*. This was applied to the AO802 suspensions only as the difference in the two pHs were quite significant, by about 1 pH unit, but not too large to be a real effect.

According to Figure 7a, there is a linear relationship for AKP30 suspensions with and without GO. The suspensions with 0.5 and 1.0 dwb % GO can be represented by the same linear relationship with an intercept value for the zeta potential of 41 mV. This relationship is, however, not obeyed in the very low yield stress region. The linear relationship obtained for the suspension without GO is less accurate due to a relatively large degree of scatter in the data but is regarded as acceptable. The intercept value of the zeta potential squared axis is larger than that previously reported[41] giving a zeta potential value ranging from 45 to 55 mV. This value is higher than that with GO meaning that a weaker network structure is formed by GO at the pH of zero zeta potential.[41] For the AO802 alumina suspensions with and without GO, linear relationships as shown in Figure 7b appeared to also describe the yield stress and zeta potential squared data. The fit, like the AKP 30, is bad for data in the low yield stress region. It appeared that the intercept value is higher for the 1.0 dwb % GO ($\sim$35mV) compared to that of ($\sim$33mV) for the 0.5 dwb % GO but the difference is too small to allow for definitive correlation between bridging strength and intercept zeta potential value. Also, the intercept value for the suspension without GO is similar in value ranging from 30 to 35 mV.

For the Alusion alumina with and without GO, a linear relationship with negative slope was also observed for 0.5 dwb % GO and that without GO as shown in Figure 7c. An intercept value for the zeta potential of $\sim$ 40 and $\sim$51 mV was obtained for that without GO and with 0.5 dwb % GO. For the 1.0 dwb % GO in Alusion alumina suspension, the data used in the fit were obtained in both the positive and negative charge region. However, there is only one point in the positive charge region due to its low pH of zero zeta potential of 2.5. The yield stress data appeared to show a maximum at 300 mV^2 or zeta potential of -15 mV (see Figure 5c). For effective particle bridging, all the carboxylic acid groups on the GO sheet must be charged and the platelet particles must have sufficient positive charges. This could explain why the maximum yield stress is located at pH 5.5 instead of 2.5 the pH of zero zeta potential (see Figure 5c). At pH 5.5, the carboxylic acid group is usually in the dissociated state. So at this pH, a given GO sheet will have sufficient charges to bridge one or more platelet Alusion alumina

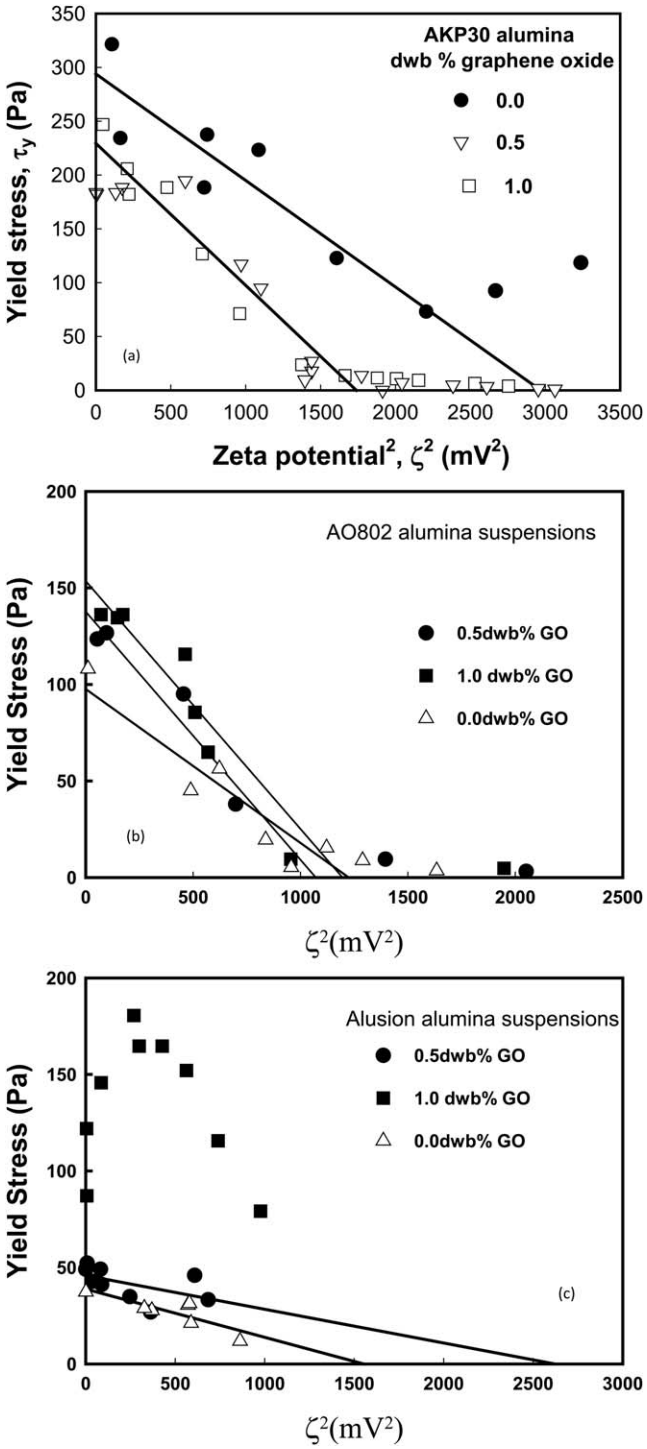

Figure 7. The plot of yield stress vs. square of zeta potential for (a) irregular AKP30, (b) spherical AO802, and (c) platelet Alusion alumina suspensions.

particles. The magnitude of the zeta potential is an indication of the strength of the repulsive interaction between the interacting particles. A zeta potential with a magnitude of 15 mV is an indication of a relatively weak repulsive interaction. Without an additive mediating the particle–particle interaction, the van der Waals attractive would have dominated the interaction with the suspension being flocculated. The maximum yield stress occurring at a zeta potential of −15 mV suggests that the number of positively charged sites on the Alusion particles must be at optimum at this point allowing effective bridging with the negatively charged GO sheets producing a flocculated suspension of maximum gel strength. The strong heterogeneous charged attraction between the GO and Alusion particles must be in the right architectural configurations to produce this large increase in the gel strength.

In summary, GO is very effective in increasing the strength of the attractive force between micron-sized platelet alumina particles via bridging. At a given solids concentration, the particle concentration will be far less than submicron-sized alumina suspension requiring much less amount of GO sheets to strengthen each particle–particle bond. Moreover, we postulate that platelet morphology of the alumina particles facilitate a much stronger interactions between the carboxylate groups located on the edge of the GO sheets and particles, that is, edge–face or edge–edge interaction (Figure 6). With submicron-sized AKP30 and AO802 alumina suspensions, the particle number concentration can be several orders of magnitude larger. There are not enough GO sheets to strengthen each interparticle bond. Moreover, a micron-sized GO sheet can have several particles adsorbed on it at the same time particularly at the edges. This type of adsorbed configuration is not directed toward increasing the interparticle attractive force of the flocculated network. Hence, this was reflected by a smaller increase or even a small decrease in the yield stress.

The structural feature of GO is still unclear and ambiguous.[17] There are several structural models of GO available in the literatures.[17] There are GO models where the —COOH group is not present.[43] Some models showed the presence of phenolic —OH group.[17] The model proposed by Lerf et al.[44] is most cited where a small amount of carboxylate groups are present along the edges of the GO sheet. The presence of this carboxylate group was indirectly supported by infrared data. The yield stress result obtained here appeared to lend further indirect support to this GO structural model with peripheral carboxylic acid groups (Figure 2d[30]). Moreover, the very low pH of the GO dispersion is also an indication of —COOH being present in addition to the other acidic group, the phenolic group. The —COOH acid is usually a much stronger acid with a pKa value of 5 compared to 10 for the phenol —OH group. We believe that this report is the first ever on GO acting as an effective bridging agent for a particular shape and size of the particles where the location of the carboxylic groups on GO is essential for producing the ideal bridging interaction observed.

Conclusions

Micron-sized GO sheets are very effective in increasing the strength of the interparticle attractive forces of micron-sized platelet alumina suspensions as reflected by the six-folds increase in the maximum yield stress of 55 wt % solids suspension at 1.0 dwb % GO. The attraction between the GO and the platelet alumina particles must be in the right architectural configurations to increase the strength of the flocculated network structure. This is, however, not true with submicron irregular and spherical shape alumina suspensions. Multiple particles adsorption on GO sheets does not normally produced a particle–particle interaction configuration that enhances the network strength especially in an environment of deficient GO. Based on dissociation constant values of —COOH and phenol —OH, we believe this is the first

result ever reported that GO layer can acts as a bridging agent caused by the interaction of the polar —COOH group, located in an ideal position to bridge with the nearest particle.

Acknowledgments

H. Husin is supported by scholarships from the Malaysian government and Universiti Tecknologi Mara. The authors wish to thank the referees for making this a better article.

Literature Cited

1. Wu JS, Pisula W, Mullen K. Graphenes as potential material for electronics. *Chem Rev*. 2007;107:718–747.
2. Zhang LL, Zhao S, Tian XN, Zhao XS. Layered graphene oxide nanostructures with sandwiched conducting polymers as supercapacitor electrodes. *Langmuir*. 2010;26:17624–17628.
3. Paulus GLC, Shimizu S, Abrahamson JT, Zhang J, Hilmer AJ, Strano MS. The chemical engineering of low-dimensional materials. *AIChE J*. 2011;57:1104–1118.
4. Mativetsky JM, Loo Y-L. Modular construction and deconstruction of organic solar cells. *AIChE J*. 2012;58:3280–3288.
5. Fang M, Long L, Zhao W, Wang L, Chen G. pH-responsive chitosan-mediated graphene dispersions. *Langmuir*. 2010;26:16771–16774.
6. Cote LJ, Kim J, Zhang Z, Sun C, Huang J. Tunable assembly of graphene oxide surfactant sheets: wrinkles, overlaps and impacts on thin film properties. *Soft Matter*. 2010;6:6096–6101.
7. Wang SJ, Geng Y, Zheng Q, Kim JK. Fabrication of highly conducting and transparent graphene films. *Carbon*. 2010;48:1815–1823.
8. Si YC, Samulski ET. Exfoliated graphene separated by platinum nanoparticles. *Chem Mater*. 2008;20:6792–6797.
9. Kim SC, Lee HI, Jeong HM, Kim BK, Kim JH, Shin CM. Effect of pyrene treatment on the properties of graphene/epoxy nanocomposites. *Macromol Res*. 2010;18:1125–1128.
10. Kuilla T, Bhadra S, Yao D, Kim NH, Bose S, Lee JH. Recent advances in graphene based composites. *Prog Polym Sci*. 2010; 35(11):1350–1375.
11. Wang L, Stuckert NR, Yang RT. Unique hydrogen adsorption properties of graphene. *AIChE J*. 2011;57:2902–2908.
12. Wang X, Zhou X, Yao K, Zhang J, Liu Z. A SnO2/graphene composite as a high stability electrode for lithium ion batteries. *Carbon*. 2011;49:133–139.
13. Fu Y, Chen H, Sun X, Wang X. Graphene-supported nickel ferrite: A magnetically separable photocatalyst with high activity under visible light. *AIChE J*. 2012;58:3298–3305.
14. Wang L, Yang RT, Sun C-L. Graphene and other carbon sorbents for selective adsorption of thiophene from liquid fuel. *AIChE J*. 2013;59:29–32.
15. Gao W, Alemany LB, Ci L, Ajayan PM. New insights into the structure and reduction of graphite oxide. *Nat Chem*. 2009;1:403–408.
16. Casabianca LB, Shaibat MA, Cai WW, Park S, Piner R, Ruoff RS, Ishii Y. NMR-based structural modeling of graphite oxide using multidimensional 13C solid-state NMR and ab initio chemical shift calculations. *J Am Chem Soc*. 2010;132(16):5672–5676.
17. Dreyer DR, Park S, Bielawski CW, Ruoff RS. The chemistry of graphene oxide. *Chem Soc Rev*. 2010;39:228–240.
18. Galande C, Mohite AD, Naumov AV, Gao W, Ci LJ, Ajayan A, Gao H, Srivastava A, Weisman RB, Ajayan PM. Quasi-molecular fluorescence from graphene oxide. *Sci Rep*. 2011;1(85):1–5.
19. Perera SD, Mariano RG, Nijem N, Chabal Y, Ferraris JP, Balkus KJ Jr. Alkaline deoxygenated graphene oxide of supercapacitor applications: an effective green alternative for chemically reduced graphene. *J Power Sources*. 2012;215:1–10.
20. Zhang WL, Choi HJ. Silica-graphene oxide hybrid composite particles and their electroresponsive characteristics. *Langmuir*. 2012;28: 7055–7062.
21. Zhang WL, Park BJ, Choi HJ. Colloidal graphene oxide/polyaniline nanocomposite and its electrorheology. *Chem Commun*. 2010;46(30): 5596–5598.
22. Zhang WL, Choi HJ. Fast and facile fabrication of a graphene oxide/titania nanocomposite and its electro-responsive characteristics. *Chem Commun*. 2011;47:12286–12288.
23. Zhang WL, Liu YD, Choi HJ. Graphene oxide coated core-shell structured polystyrene microspheres and their electrorheological characteristics under applied electric field. *J Mater Chem*. 2011;21: 6916–6921.
24. Leong YK, Scales PJ, Healy TW, Boger DV, Buscall R. Rheological evidence of adsorbate-mediated short-range steric forces in concentrated dispersions. *J Chem Soc Faraday Trans*. 1993;89(14): 2473–2478.
25. Leong YK, Scales PJ, Healy TW, Boger DV. Interparticle forces arising from adsorbed polyelectrolytes in colloidal suspensions. *Colloids Surf A*. 1995;95(1):43–52.
26. Leong YK, Scales PJ, Healy TW, Boger DV. Effect of particle size on colloidal zirconia rheology at the isoelectric point. *J Am Ceram Soc*. 1995;78(8):2209–2212.
27. Khoo KS, Teh EJ, Leong YK, Ong BC. Hydrogen bonding and interparticle forces in platelet α-Al2O3 dispersions: Yield stress and zeta potential. *Langmuir*. 2009;25(6):3418–3424.
28. Hummers WS, Offeman RE. Preparation of graphitic oxide. *J Am Chem Soc*. 1958;80:1339.
29. Liang JJ, Huang Y, Zhang L, Wang Y, Ma YF, Guo TY, Chen YS. Molecular-level dispersion of graphene into poly(vinyl alcohol) and effective reinforcement of their nanocomposites. *Adv Funct Mater*. 2009;19(14):2297–2302.
30. Hamilton CE. Functionalization, Coordination and Coating of Carbon Nanotubes. Ph.D. Thesis, Rice University, 2009.
31. Stankovich S, Dikin DA, Dommett GHB, Kohlhaas KM, Zimney EJ, Stach EA, Piner RD, Nguyen ST, Ruoff RS. Graphene-based composite materials. *Nature*. 2006;442(7100):282–286.
32. Konkena B, Vasudevan S. Understanding aqueous dispersibility of graphene oxide and reduced graphene oxide through pKa measurements. *J Phys Chem Lett*. 2012;3:867–872.
33. Wang X, Bai H, Shi G. Size fraction of graphene oxide sheets by pH-assisted selective sedimentation. *J Am Chem Soc*. 2011;133: 6338–6342.
34. Leong YK. Particle bridging in dispersions by small charged molecules: chain length and rigidity, architecture and functional groups spatial position. *Phys Chem Chem Phys*. 2007;9:5608–5618.
35. Leong YK. Role of molecular architecture of citric and related polyacids on the yield stress of α-alumina slurries: inter- and intramolecular forces. *J Am Ceram Soc*. 2010;93:2598–2605.
36. Teh EJ, Leong YK, Liu Y. Isomerism and solubility of benzene mono- and dicarboxylic acid: its effect on alumina dispersions. *Langmuir*. 2011;27(1):49–58.
37. Husin H, Leong YK, Liu J. The effects of benzoic acid compounds in α-Al2O3 dispersions: additional attractive forces of particle bridging and precipitate bridging. *Colloids Surf A*. 2012;402:159–167.
38. Larson LG. The Structure and Rheology of Complex Fluids. New York: Oxford University Press, 1999.
39. Teh EJ, Leong YK, Liu Y, Ong BC, Berndt CC, Chen SB. Yield stress and zeta potential of washed and highly spherical oxide dispersions-critical zeta potential and hamaker constant. *Powder Technol*. 2010;198:114–119.
40. Jayaweera P, Hettiarachchi S, Ocken H. Determination of the high temperature zeta potential and pH of zero charge of some transition metal oxides. *Colloids Surf A*. 1994;85(1):19–27.
41. Ramakrishnan V, Pradip, Malghan SG. The stability of alumina-zirconia suspensions. *Colloids Surf A*. 1998;133(1-2):135–142.
42. Ong BC, Leong YK, Chen SB. Yield stress-zeta potential relationship of oxide dispersions with adsorbed polyacrylate-Steric effect and zeta potential at the flocculated-dispersed transition state. *Powder Technol*. 2008;186:176–183.
43. Szabo T, Berkesi O, Forgo P, Josepovits K, Sanakis Y, Petridis D, Dekany I. Evolution of surface functional groups in a series of progressively oxidized graphite oxides. *Chem Mater*. 2006;18: 2740–2749.
44. Lerf A, He HY, Forster M, Klinowski J. Structure of graphite oxide revisited. *J Phys Chem B*. 1998;102(23):4477–4482.

Manuscript received Dec. 5, 2012, and revision received Mar. 12, 2013.